

JGR Solid Earth

RESEARCH ARTICLE

10.1029/2020JB020745

Key Points:

- A 3-D high-precision relocation method is explored using multiple phases
- Accurate estimates are generated for the burial depths of the North Korean nuclear tests
- The yield is estimated to be 225.7 kt for the largest nuclear explosion at the North Korea test site based on a data-constrained burial depth of 570 m

Supporting Information:

Supporting Information may be found in the online version of this article.

Correspondence to:

L. F. Zhao,
zhaolf@mail.iggcas.ac.cn


Citation:

Yang, G., Zhao, L. F., Xie, X. B., Zhang, L., & Yao, Z. X. (2021). High-precision relocation with the burial depths of the North Korean underground nuclear explosions by combining Pn and Pg differential traveltimes. *Journal of Geophysical Research: Solid Earth*, 126, e2020JB020745. <https://doi.org/10.1029/2020JB020745>

Received 9 AUG 2020

Accepted 30 MAY 2021

High-Precision Relocation With the Burial Depths of the North Korean Underground Nuclear Explosions by Combining Pn and Pg Differential Traveltimes

G. Yang^{1,2}, L. F. Zhao^{1,3} , X. B. Xie⁴, L. Zhang^{1,2}, and Z. X. Yao¹

¹Key Laboratory of Earth and Planetary Physics, Institute of Geology and Geophysics, Chinese Academy of Sciences, Beijing, China, ²College of Earth and Planetary Sciences, University of Chinese Academy of Sciences, Beijing, China, ³Mohe Observatory of Geophysics, Institute of Geology and Geophysics, Chinese Academy of Sciences, Beijing, China, ⁴Institute of Geophysics and Planetary Physics, University of California at Santa Cruz, Santa Cruz, CA, USA

Abstract In seismic nuclear monitoring, an accurate source depth is an important prerequisite for reliably estimating the explosive yield. Relative location methods are often used for this purpose. However, the conventional method based on regional Pn waves usually fails to give satisfactory constraints on the source depth, mainly due to the strong trade-off between the burial depth and origin time. This study explores a high-precision relative location method to simultaneously determine the relative epicenter and source elevation by using differential traveltimes from both downward-takeoff Pn waves and horizontal-takeoff Pg waves. The properties of both Pg and Pn waves, including the consistency between waveforms, the reliability of differential traveltime measurements, and their sensitivities to epicenter and depth variations, are investigated. By jointly applying both types of waveform data, the proposed method significantly enhances the constraint on the source depth variation. This method is applied to regional seismic data collected from China, South Korea, and Japan to determine the relative epicenters, origin times and relative burial depths of six North Korean underground nuclear explosions. The source depths are then used to provide burial-depth corrections to estimate the explosive yields. The depths of the six North Korean nuclear explosions detonated on October 2006, May 2009, February 2013, January 2016, September 2016, and September 2017 are determined to be 330, 540, 506, 468, 521, and 570 m, respectively, and their yields after burial depth corrections are 1.6, 5.7, 13.4, 12.6, 21.7, and 225.7 kt, respectively.

Plain Language Summary For many years, the issue of nuclear testing has been a concern throughout the international community. The 1996 Comprehensive Nuclear-Test-Ban Treaty stipulated that radioactive, infrasound, seismic wave and underwater acoustic detection techniques can be used to monitor nuclear testing. From October 9, 2006 to September 3, 2017, the Democratic People's Republic of Korea conducted six underground nuclear tests whose locations, origin times and explosive yields have been estimated by numerous studies. Among these parameters, the determination of the burial depth of a nuclear test is always particularly difficult yet nevertheless crucial, being a prerequisite to reasonably estimate the explosive yield. Seismological relative location methods determine locations of earthquakes relative to a master reference event by comparing differences in seismic wave propagation times between earthquakes to be determined and the master event. In a large number of previous studies, relative location methods based on one kind of seismic wave often encounter difficulties to determine the burial depth. Therefore, in this study, we explore a multiple seismic wave relocation method to simultaneously determine the surface location and burial depth of underground nuclear explosions. Additionally, we re-estimate the explosive yields of the North Korean nuclear tests by incorporating the refined burial depths.

1. Introduction

Since 2006, North Korea has conducted six underground nuclear tests. The United States Geological Survey (USGS) reported body-wave magnitudes of 4.3, 4.7, 5.1, 5.1, 5.3, and 6.3 for the events on October 9, 2006, May 25, 2009, February 12, 2013, January 6 and September 9, 2016, and September 3, 2017, respectively. The six nuclear tests at the North Korea test site (NKTS) are hereafter referred to as NKT1, 2, 3, 4, 5, and 6 in chronological order. Many researchers have studied the epicenter locations, burial depths, origin times, magnitudes, and yields of these six events; in particular, however, it is often difficult yet crucial to accurately

estimate the burial depth as a result of the shallow burial, the lack of nearby stations, and the uncertainty in the underground structure. Moreover, an accurate overburden thickness is a prerequisite for correctly determining the explosion yield because of the strong trade-off between the yield and depth. For example, in previous studies, by assuming normally scaled burial depths, the yields of NKT1-5 were estimated to be 0.5, 2.4, 7.5, 4.0, and 6.0 kt based on Lg-wave magnitude-yield empirical relations (Bowers et al., 2001; Murphy, 1996; Nuttli, 1986; Ringdal et al., 1992; Zhao et al., 2016, 2017). However, after implementing burial depth corrections based on surface elevation differences, these yields were re-estimated to be 1.0, 6.0, 12.0, 9.0, 16.0, and 72.0 kt (Xie & Zhao, 2018), significantly larger than those without considering the depth effect. Pasyanos and Myers (2018) suggested that NKT6 had a maximum yield of 130–150 kt at a possible burial depth of approximately 600 m. Voytan et al. (2019) estimated the yields of NKT1-6 to be 1.4, 5.0, 13.2, 11.2, 18.8, and 250.0 kt by giving burial depths based on a 4% tunnel slope assumption. Evidently, without reliable burial depth data, the yield estimate could involve great uncertainties.

Various methods, such as the spectral ratio analysis method (Murphy et al., 2010, 2013), hydrodynamic calculation method (Rougier et al., 2011) and regional waveform envelope method (Pasyanos & Ford, 2015; Pasyanos & Myers, 2018; Pasyanos et al., 2012), have been explored by different authors to determine the burial depth of an underground nuclear test. Interferometric synthetic aperture radar (InSAR) surface displacement data obtained at the NKTS could also constrain the burial depths, epicenters and yields of these six events (Wei, 2017; Myers et al., 2018; Sreejith et al., 2020; Wang et al., 2018). In addition, the burial depth may be roughly estimated by the surface elevation difference between the associated tunnel entrance and the epicenter (e.g., Tian et al., 2018; Voytan et al., 2019; Zhang & Wen, 2013). Relative location methods have frequently been used to provide accurate epicenters relative to a reference event for a group of closely distributed sources such as aftershock sequences or nuclear explosions. Accordingly, this approach has been successfully applied to obtain the relative locations of the NKTS nuclear explosions (e.g., Gibbons et al., 2017; He et al., 2018; Murphy et al., 2013; Schaff et al., 2018; Selby, 2010; Tian et al., 2018; Tibuleac et al., 2008; Wen & Long, 2010; Zhang & Wen, 2013; Zhao et al., 2014, 2016, 2017). However, most of these relative location methods do not provide satisfactory information on the burial depth due to the strong trade-off between the burial depth and origin time (e.g., Waldhauser & Ellsworth, 2000; Zhao et al., 2014). The above disadvantage results mainly from the fact that, traditionally, only Pn waves were used in relative locations at regional distances. However, if Pg waves can be combined with Pn waves, they can jointly provide a broad takeoff angle coverage and better constrain the source location, including both the epicenter and the focal depth.

Multiple phases have been employed to constrain epicenters and source depths. In this context, Greensfelder (1965) proposed a method to determine earthquake depths based on the difference between Pn and Pg traveltimes recorded at the same station; this method was successfully applied to estimate the source depths of earthquakes in Nevada. By using different combinations of Pg, Pn, and PmP arrival times, Wagner et al. (2013) determined focal depths both from a synthetic data set and from the data of four real earthquakes in the northern Alpine foreland. More recently, a relative location method combining Pn and Pg phases was successfully applied to the Jiuzhaigou earthquake in China to estimate the depth where the rupture initiated (Wei et al., 2019).

In this study, we explored a high-precision relative location method to determine relative epicenters and relative burial depths using differential traveltimes (DTTs) from both Pn and Pg waves. With this method and seismic data collected from the Global Seismic Network (GSN), China National Digital Seismic Network (CNDSN) and Full-Range Seismograph Network (F-net), we investigated the epicenters, origin times and burial depths of the six NKTS nuclear tests (Figure 1). Additionally, the yields of these six NKTS nuclear explosions were re-estimated based on an empirical magnitude-yield relation (Bowers et al., 2001; Patton & Taylor, 2011) for standard scaled burial depths plus corrections calculated using the source depths estimated in this study.

2. Methodology for Determining 3-D Relative Locations

Precisely estimating the epicenter of an event requires a station distribution with good azimuthal coverage. Similarly, to effectively constrain the source depth in the vertical direction, a good takeoff angle coverage is needed. Traditionally, at regional distances, only Pn waves were used to determine relative locations,

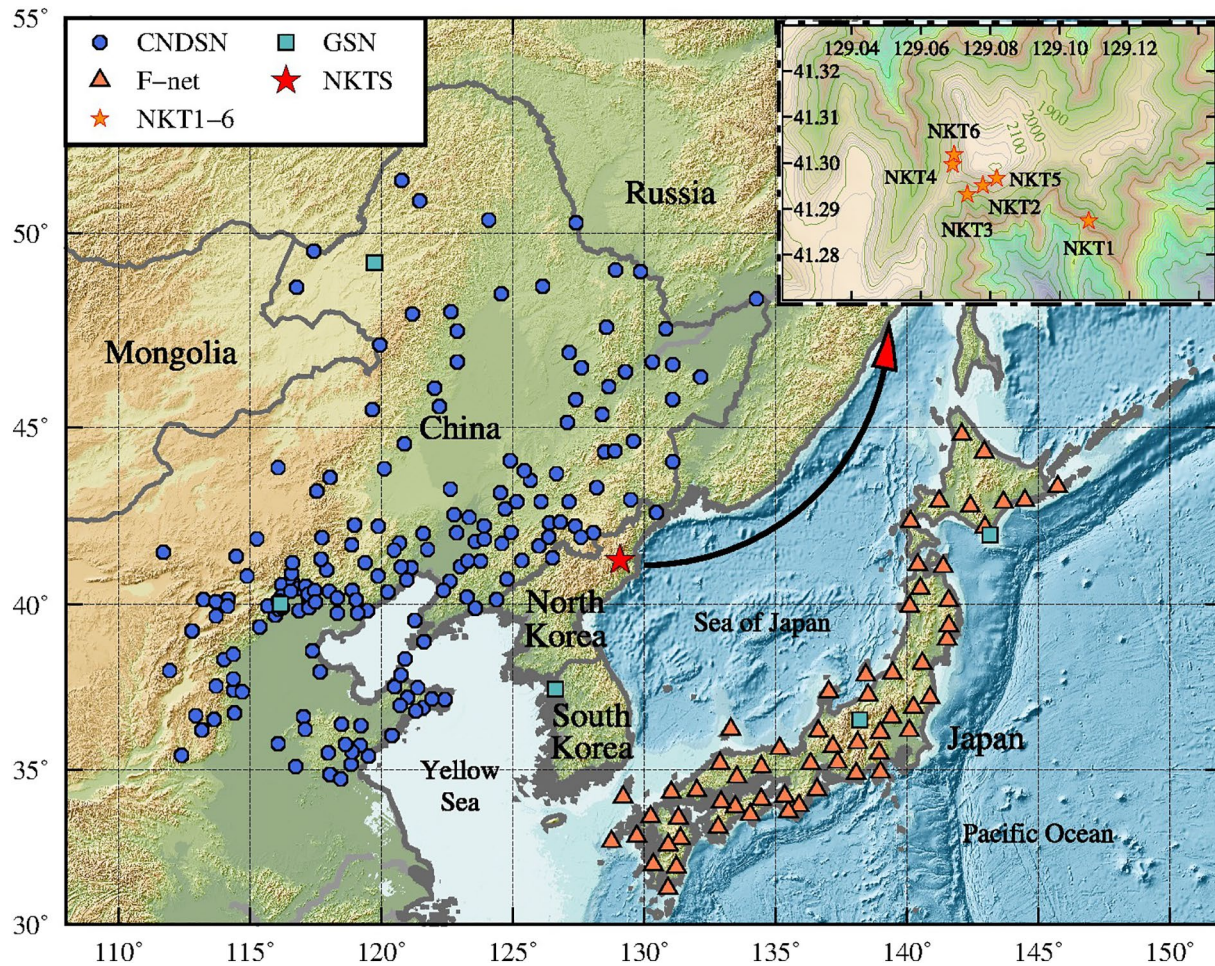


Figure 1. Map showing the locations of the North Korea test site (NKTS, red star) and the stations used in this study, including those from the China National Digital Seismic Network (CNDSN, blue circles), Global Seismic Network (GSN, green squares) and Full-Range Seismograph Network (F-net, red triangles). The inset map in the upper-right corner illustrates the locations of the six NKTS nuclear tests (red stars) reported by He et al. (2018).

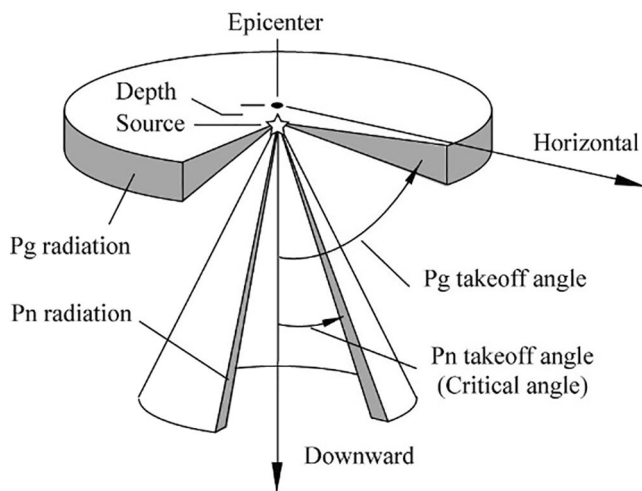


Figure 2. Sketch showing the radiation of Pg and Pn waves from a shallow source. The shaded areas indicate the takeoff angle ranges for both waves.

mainly because they are first arrivals and are thus less contaminated than subsequent arrivals. However, the Pn wave has a takeoff angle, with all rays from a source forming a conical surface with an opening angle that is twice the P-wave critical angle at the Moho discontinuity. Figure 2 is a sketch showing the radiation directions of the Pn and Pg waves from a shallow source. Because all Pn rays radiate downward within a small angular range, the Pn traveltimes are sensitive to the source depth. However, the generally downward radiation of Pn waves leads to a strong trade-off between the origin time and source depth, making it difficult to use Pn waves alone to determine the source depth, even when using stations with good azimuthal coverage. In contrast, crustal Pg waves leave the source at a nearly horizontal takeoff angle (Figure 2). Hence, while Pg waves are weakly sensitive to the source depth (Campillo et al., 1984), they provide good constraints on the epicenter and origin time if stations with a good azimuthal coverage are available. Consequently, if Pg and Pn waveform data can be combined, they can jointly provide a more complete takeoff angle coverage and better constraints on the source location, including both the epicenter and the focal depth.

The propagation of a Pg wave is more complicated than that of a Pn wave. In the crust with a vertical velocity gradient, Pg waves are considered to propagate along turning rays bouncing between the free surface and their deepest turning points. On the other hand, according to coda wave theory (Sato & Fehler, 1998), the early parts of Pg waves are mostly direct arrivals, while their later parts are composed of multiple scattered waves; the real situation is likely between these two extremes. Low-frequency Pg energy propagates along a stable turning raypath; then, with increasing frequency, these turning rays split, forming a more complex and diversified ray system reverberating within the upper or even the entire crust. At even higher frequencies, the Pg is dominated by scatterings caused by small-scale random heterogeneities in the crust. Therefore, observed Pg waves usually have complicated takeoff angles, and their properties vary with both the frequency and the group velocity.

For nuclear explosions whose burial depths are much smaller than the epicentral distance, it is reasonable to consider low- to moderate-frequency Pg waves propagating nearly horizontally. Therefore, the Pg traveltimes are far less sensitive to the burial depth than the Pn traveltimes but offers good constraints on the epicenter and the origin time. On the other hand, the Pn traveltimes are sensitive to the source depth but requires additional information on the origin time to determine the burial depth. Both datasets are compensated and relatively decoupled regarding the source depth. Therefore, it is expected that combining Pg and Pn waveform data can improve the takeoff angle coverage and significantly enhance the source depth constraint (Wagner et al., 2013; Wei et al., 2019).

Before confidently using Pg wave traveltimes for relative location, we investigated the properties of these waves. We first evaluated the correlations of Pg waveforms originating from closely located sources within different frequency bands and group velocity windows. Figure 3a illustrates the cross-correlation results of Pn and Pg waves between NKT4 and NKT5 recorded at station JL.CN2 (epicentral distance is approximately 408.3 km) within three frequency bands, 1.0–4.0, 2.0–5.0, and 3.0–6.0 Hz, where R and T are the cross-correlation coefficients and DTTs, respectively, of the Pn (red) and Pg (blue) waves. Due to the consistency among the focal mechanisms and the closeness of the epicenters of the two explosions, the Pn and Pg waveforms both appear to be highly correlated. Compared with those of the Pn wave, the correlation coefficients of the Pg wave are slightly lower and decrease with increasing frequency but still meet the quality requirements for measuring the DTT using cross-correlation. To balance both the waveform consistency and the measurement accuracy, we employed the 2.0–5.0 Hz frequency band for all DTT measurements hereafter.

Theoretically, the DTT is dependent only on the relative locations of two sources, the leaving directions of signals, and the near-source velocity. However, the complicated Pg wave takeoff angle may cause errors in DTT measurements. Figure 3b illustrates the measured DTTs between NKT4 and NKT5 recorded at selected stations. They are calculated using cross-correlations in a 0.2-km/s-long group velocity window moving from 6.3 to 5.4 km/s. The solid circles are at different group velocities with their color shades represent their correlation coefficients, and the dashed lines indicate the DTTs calculated within a longer group velocity window between 6.3 and 5.4 km/s. By investigating measurements at different group velocities, we see that the DTTs at shorter epicentral distances and larger group velocities (earlier part) appear to be more consistent, with circles close to the average values and have smaller rms values. The DTTs from later Pg tends to be more scattered, which may be resulted from that the takeoff angles and wave paths of the later Pg are more diversified. To reduce the fluctuations, we choose to use a group velocity window between 6.3 and 5.4 km/s (the shaded area) to measure the DTT, which is equivalent to take the average of all circles.

To further investigate the sensitivity of Pn and Pg DTTs to the source depth and the feasibility of using them for depth location, we selected two event pairs for statistical analysis with their results shown in Figure 3c. DTTs of Pn and Pg waves can be expressed as

$$\Delta t_{Pn} = \frac{\Delta x}{v_{Pn}} + A\Delta h + t_0 \quad (1)$$

and

$$\Delta t_{Pg} = \frac{\Delta x}{v_{Pg}} + B\Delta h + t_0, \quad (2)$$

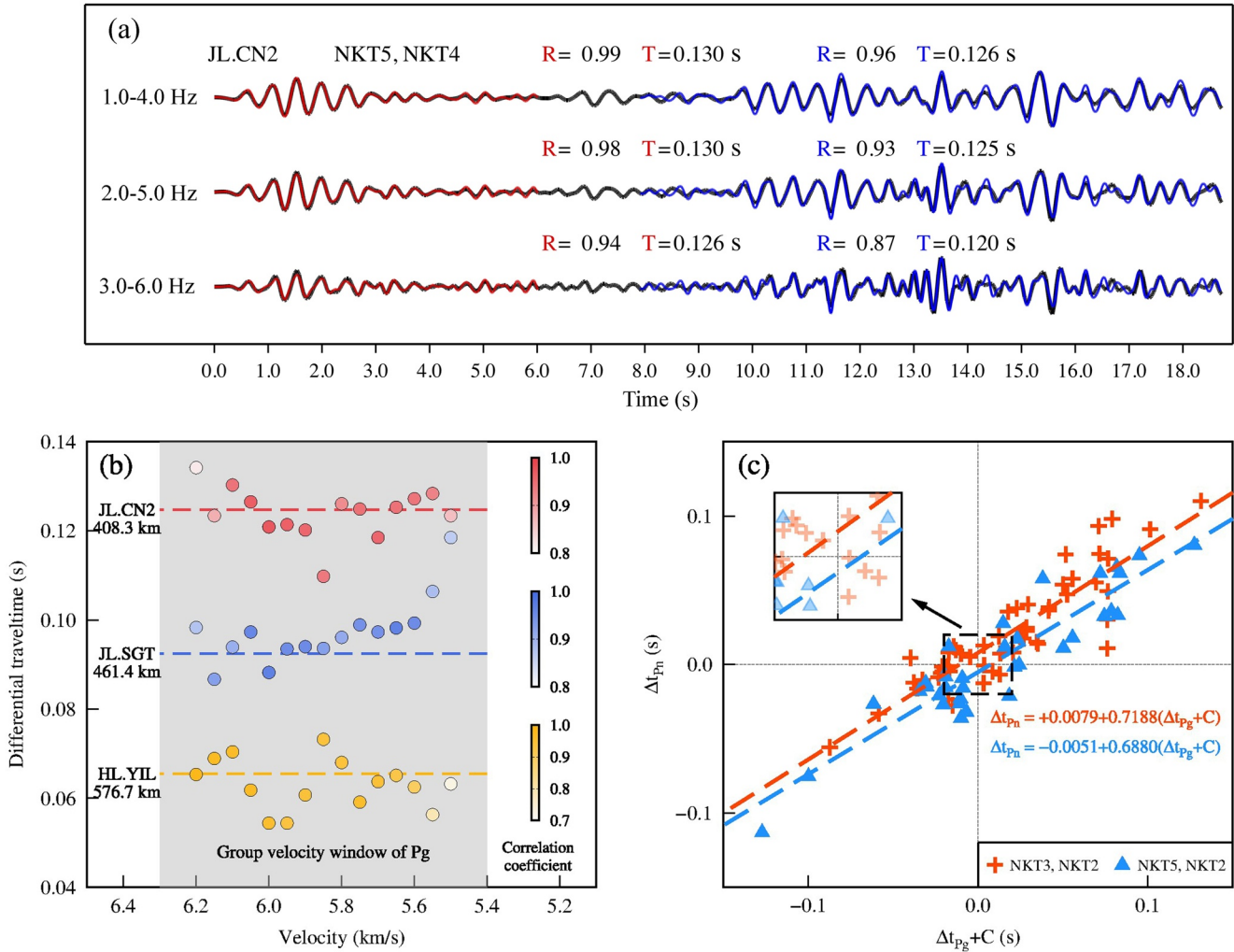


Figure 3. Analyses of the Pg wave properties. (a) Cross-correlations of Pn (red) and Pg (blue) waves in different frequency bands. (b) Pg differential traveltime (DTT)s between NKT4 and NKT5 versus the group velocities at three stations. The solid circles are values at different group velocities, and the dashed lines indicate the average DTTs calculated in the 6.3–5.4 km/s velocity window. (c) Pn DTTs versus the Pg DTTs corrected for the influence of the epicenter difference term $C = \Delta x \left(\frac{1}{v_{Pn}} - \frac{1}{v_{Pg}} \right)$ for event pair NKT3 and NKT2 and event pair NKT5 and NKT2. The best fitting lines are labeled in the figure with an enlarged view (inset) showing their interceptions.

where Δx is the distance difference between the two epicenters, and A and B are coefficients how the depth difference affecting the DTTs. Subtracting Equation 2 from Equation 1 to eliminate the origin time t_0 , we have

$$\Delta t_{Pn} = (\Delta t_{Pg} + C) + (A - B)\Delta h, \quad (3)$$

where $C = \Delta x \left(\frac{1}{v_{Pn}} - \frac{1}{v_{Pg}} \right)$ is the contribution from the epicenter difference. If Pg and Pn waves have similar takeoff angles, A approaches to B . The difference $(A - B)$ is nearly zero and the Δt_{Pn} versus $(\Delta t_{Pg} + C)$ is a linear equation passing through the origin. In Figure 3c, the lines fitted by real data show apparent interceptions, which provide constrains on relative elevation between two sources. The depth term corresponding to the intercept between NKT3 and NKT2 is approximately 51% of the epicentral term, which is unlikely a trivial value caused by errors.

The above analyses reveal that the Pg waves from two close shallow explosion sources are highly correlated even with the complex propagation mechanism. Their DTTs can be properly measured using the cross-correlation method. Combining both Pn and Pg data can provide constrain on the relative source depth.

Based on the above analysis and previous studies (e.g., Gibbons et al., 2017; He et al., 2018; Murphy et al., 2013; Myers et al., 2018; Schaff et al., 2018; Selby, 2010; Tian et al., 2018; Tibuleac et al., 2008; Wen & Long, 2010; Zhang & Wen, 2013; Zhao et al., 2014, 2016, 2017), we constructed a relative location system based on the DTTs from both Pg and Pn waves

$$As = d, \quad (4)$$

where $s = (x, y, t_0, h)^T = (s_1, h)^T$; $s_1 = (x, y, t_0)^T$; x, y, t_0 , and h are vectors composed of the longitudes, latitudes, origin times and depths, respectively, of a group of seismic events to be determined, and the superscript T denotes the transpose. $d = (\Delta T_{Pg}, \Delta T_{Pn})^T$ is a vector composed of the observed DTTs ΔT_{Pg} and ΔT_{Pn} of Pg and Pn waves, respectively. The matrix

$$A = \begin{bmatrix} a_{Pg,S} & a_{Pg,h} \\ a_{Pn,S} & a_{Pn,h} \end{bmatrix} \quad (5)$$

is composed of coefficients reflecting how the Pg and Pn DTTs depend on the source locations, origin times, and local velocities (Waldhauser & Ellsworth, 2000). Combining these terms together, we have

$$\begin{bmatrix} a_{Pg,S} & a_{Pg,h} \\ a_{Pn,S} & a_{Pn,h} \end{bmatrix} \begin{bmatrix} s_1 \\ h \end{bmatrix} = \begin{bmatrix} \Delta T_{Pg} \\ \Delta T_{Pn} \end{bmatrix}. \quad (6)$$

In general, the Pg and Pn DTTs have different numbers of data points and measurement qualities, and these differences may affect the relative locations in different ways. Certain weights can be applied to the system:

$$wAs = wd, \quad (7)$$

where

$$w = \begin{bmatrix} eI_{Pg} & 0 \\ 0 & (1-e)I_{Pn} \end{bmatrix}$$

is the weighting matrix, e is the weighting function, and I_{Pg} and I_{Pn} are unit matrixes having the same size as the Pg and Pn data vectors, respectively. Equations 6 and 7 provide a joint inversion system to constrain the relative locations $s = (x, y, t_0, h)^T$ with both Pg and Pn data.

As mentioned earlier, if assuming the Pg waves are radiated nearly horizontally, the source depth h will be independent of the Pg DTT; thus, $a_{Pg,h} = 0$. Under this approximation, we can decouple Equation 3 into a two-step format

$$a_{Pg,S}S_1 = \Delta T_{Pg} \quad (8)$$

and

$$a_{Pn,h}h = (\Delta T_{Pn} - a_{Pn,S}S_1^{Pg}). \quad (9)$$

We first use the Pg data to solve Equation 8 to obtain the epicenter and origin time s_1^{Pg} . Then, the result is substituted into Equation 9 to determine the source depth h . To solve the joint inversion system in Equation 6 or the two-step system composed of Equations 8 and 9, the simulated annealing method (Kirkpatrick et al., 1983) is used to minimize the L2 norm between the synthetic and observed DTTs. The two objective functions for the Pg and Pn data are as follows:

$$O_{Pg}(\mathbf{x}, \mathbf{y}, \mathbf{t}_0) = \frac{1}{N(M-1)} \left\{ \sum_{k=1}^{M-j} \sum_{j=1}^{M-1} \sum_{i=1}^N \left[\Delta t_{Pg,j,j+k}^i + \Delta t_{j,j+k}^0 - \Delta T_{Pg,j,j+k}^i \right]^2 \right\}^{1/2}, \quad (10)$$

and

$$O_{Pn}(\mathbf{x}, \mathbf{y}, \mathbf{h}, \mathbf{t}_0) = \frac{1}{N(M-1)} \left\{ \sum_{k=1}^{M-j} \sum_{j=1}^{M-1} \sum_{i=1}^N \left[\Delta t_{Pn,j,j+k}^i + \Delta t_{j,j+k}^0 + \Delta t_{j,j+k}^h - \Delta T_{Pn,j,j+k}^i \right]^2 \right\}^{1/2} \quad (11)$$

where $\Delta t_{Pn,j,j+k}^i$ and $\Delta t_{Pg,j,j+k}^i$ are the synthetic DTTs of Pn and Pg waves, respectively, between events j and $j+k$ at station i ; $\Delta t_{j,j+k}^0$ denotes the difference in the origin times; $\Delta T_{Pn,j,j+k}^i$ and $\Delta T_{Pg,j,j+k}^i$ are the observed DTTs of Pn and Pg waves, respectively, between events j and $j+k$ at station i ; M and N are the numbers of events and stations, respectively; and $\Delta t_{j,j+k}^h$ represents the synthetic DTTs caused by the burial depth difference $\Delta h_{j,j+k}$:

$$\Delta t_{j,j+k}^h = \Delta h_{j,j+k} \left(-\frac{1}{\cos i_1 v_{p1}} + \frac{\tan i_1}{v_{pn}} \right), \quad (12)$$

where i_1 is the takeoff angle of Pn waves, v_{p1} is the near-surface P -wave velocity at the NKTS, and v_{pn} is the upper mantle P -wave velocity.

According to the inversion of Pg and Pn data from the NKTS, both the joint inversion and the two-step inversion yield very similar results, indicating that the Pg data are largely independent of the source depth.

3. High-Precision Relative Locations

In this section, we invert for the relative epicenters, origin times and relative burial depths of the six NKTS nuclear tests.

3.1. Regional Data and Waveform Cross-Correlation

We established a regional seismic network by incorporating 249 stations deployed across China, South Korea and Japan. From these stations, we manually selected high-quality Pn and Pg vertical component waveform data. We first removed the instrument responses from the data and bandpass-filtered them between 2.0 and 5.0 Hz. The Pn and Pg waveforms were used to calculate the DTTs between events through a waveform cross-correlation technique (Schaff et al., 2018; Schaff & Richards, 2004), where the time window of the Pn phase is 6 s and the Pg group velocity window is 6.3–5.4 km/s. A total of 945 high-quality Pn wave DTTs (Table S1) and 826 Pg wave DTTs (Table S2) were manually screened. Due to its small magnitude, unique near-source structure and larger distances to other events, NKT1 did not have sufficient amount of high-quality DTTs. Therefore, NKT1 did not participate in the inversion. Instead, we used NKT2 as the master event based on the following considerations. First, the NKT2 appears directly associated with the western tunnel entrance, providing a clue on its possible depth and its epicenter is strongly constrained by NKT1 according to He et al. (2018). Second, the location of the NKT2 is close to the geometrical center of all six events, making its waveforms better correlated with those from other events. On the other hand, as a small explosion, the NKT1 tends to produce localized surface damage above the source, making its absolute epicenter can be obtained, even did not being included in the inversion. Therefore, it is a better choice using the NKT2 as the master event. Taking stations MDJ and BEP (with epicentral distances of 372 and 701 km, respectively) as examples, Figure 4 shows the cross-correlation results for the six nuclear tests, where R and T are the cross-correlation coefficients and DTTs, respectively, of the Pn (red) and Pg (blue) waves. Due to their highly consistent focal mechanisms, very closed epicenters and nearly identical propagation paths, the waveforms from the last five events are highly correlated. However, their correlations with NKT1 are slightly lower because of larger distances.

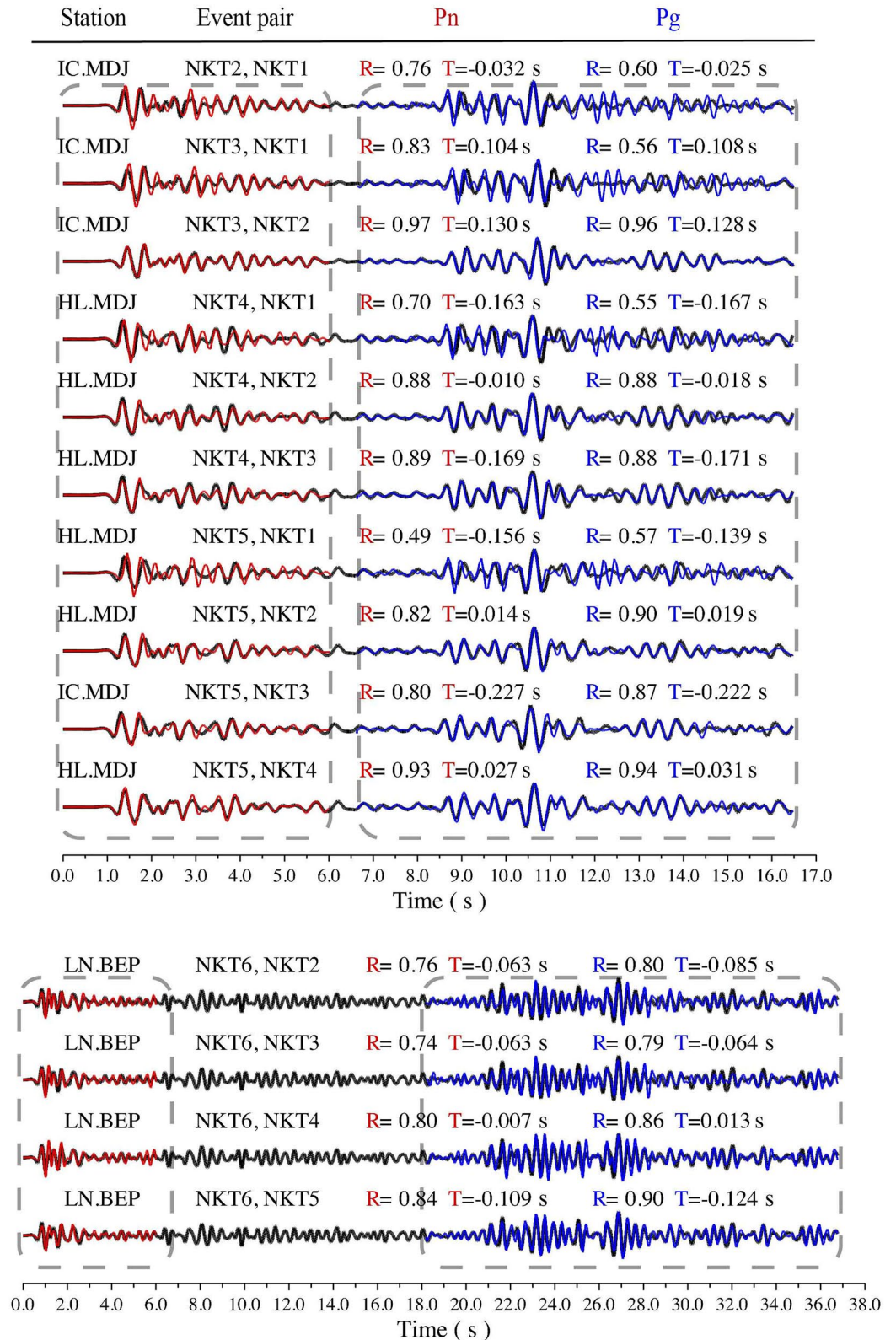


Figure 4. Vertical component waveform cross-correlation results of the Pn and Pg waves at stations MDJ and BEP. These waveforms were bandpass-filtered between 2.0 and 5.0 Hz. The epicentral distances to stations MDJ and BEP are approximately 372 and 701 km, respectively. The names of the events, cross-correlation coefficients (R) and differential traveltimes (T) of the Pn (red) and Pg (blue) waves are listed above the waveforms.

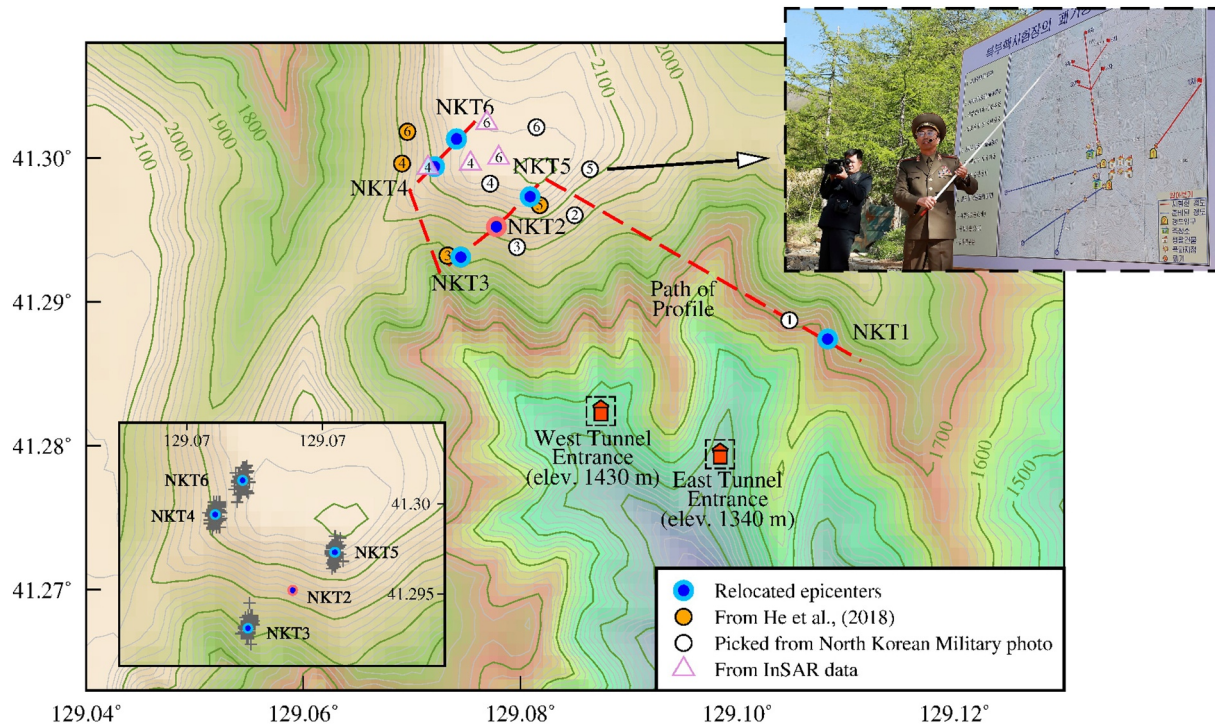


Figure 5. Map showing the topography and relocated epicenters of the North Korea test site (NKTS) nuclear explosions (solid blue circles) relative to the master event NKT2 (red solid circle). Due to the lack of Pg data, NKT1 was not included in the inversion. The yellow and white solid circles represent the epicenters provided by He et al. (2018) and the North Korean military (picked from the inset photo at the upper right), with the numbers in these circles indicating their chronological order. The numbered white triangles represent the absolute epicenters of NKT4 and NKT6 obtained from InSAR data (Wei, 2017; Myers et al., 2018; Sreejith et al., 2020; Wang et al., 2018). Two possible tunnel entrances are located south of the NKTS. The red dashed line illustrates the manually chosen path through the six nuclear tests to exhibit their relative depths (Figure 6). The relocation errors are shown in the inset map at the bottom left.

3.2. Simulated Annealing Inversion

We chose NKT2 located at (41.2952°N, 129.0778°E) (He et al., 2018) as the master event to determine the relative epicenters, relative burial depths and origin times of the last four underground nuclear tests using the relative location method described in the last section. The Pn-wave velocity in the upper mantle was fixed at 8.0 km/s (Zhao et al., 2016), and the near-surface P-wave velocity at the NKTS was estimated to be 5.2 km/s according to the Korean seismic model in the neighboring area (Bonner et al., 2008; Herrmann et al., 2005). This velocity was used to convert the inverted time variables into interevent distances. As mentioned in the Methodology section, we separated the location procedure into two steps. In the first step, we applied simulated annealing to minimize the objective function Equation 8 composed of the Pg data. A large search range was used to guarantee convergence to the global minimum: the epicenters were limited to an area of $40 \times 40 \text{ km}^2$, and the search range of the origin time was $\pm 20 \text{ s}$. The inverted epicenters and origin times of NKT3-6 are shown in Figure 5 and listed in Table 1. As illustrated in Figure 5, NKT1 was detonated at the southeast end of the NKTS and at a low elevation (Wen & Long, 2010), while NKT3-6 were relocated to the west and on the southwest slope of Mount Mantap at relatively high elevations, in agreement with the findings of previous studies (e.g., Gibbons et al., 2017; He et al., 2018; Myers et al., 2018). The epicenters of NKT2, NKT3, and NKT5 were approximately 2.7 km northwest of NKT1, while those of NKT4 and NKT6 were relocated 700 m northwest of NKT2.

With the epicenters and origin times determined by the Pg data, the second step utilizes the Pn data to constrain the relative burial depths. To provide reference burial depths for NKT1 and NKT2, we assumed that the tunnel is straight and has a slope of approximately 4% to ensure drainage (Sinha, 1991). This slope value has been adopted in other studies (e.g., Wei, 2017; Pasyanos & Myers, 2018; Voytan et al., 2019). The west and east tunnel entrances estimated by satellite photos were found at (41.2826°N, 129.0874°E) and

Table 1
Best-Fit Epicenter Locations and Origin Times of the North Korean Nuclear Tests

Event code	Date (yyyy/mm/dd)	Origin time (hh/mm/ss)	Standard deviation (s)	Latitude (°N)	Longitude (°E)	Relative location uncertainty ^e (m)
NKT1 ^a	2006/10/09	01:35:28.0000 ^b	—	41.2874 ^c	129.1083 ^c	—
NKT2	2009/05/25	00:54:43.1409 ^d	Master event	41.2952 ^d	129.0778 ^d	Master event
NKT3	2013/02/12	02:57:51.2832	0.0043	41.2931	129.0745	89
NKT4	2016/01/06	01:30:00.8695	0.0048	41.2994	129.0721	83
NKT5	2016/09/09	00:30:01.3816	0.0047	41.2973	129.0809	84
NKT6	2017/09/03	03:30:01.6188	0.0057	41.3013	129.0741	98

^aNKT1, the first North Korean nuclear test. ^bfrom the USGS. ^cfrom satellite images (Wen & Long, 2010; Zhao et al., 2014). ^dfrom relative location (He et al., 2018). ^ethe major axis of error ellipse of epicenters calculated by randomly selecting 80% of the data in each inversion (Efron, 1983).

(41.2796°N, 129.0984°E) with elevations of 1,430 m and 1,340 m, respectively (Figure 5). Therefore, we fixed the burial depths of NKT1 and NKT2 at 330 and 540 m, respectively, and chose 1,498 m (NKT2) above sea level as the reference plane. The search range for the relative elevation was ± 1 km, and the burial depths were obtained by considering the surface elevation. The convergence during the simulated annealing inversion is illustrated in Figure 6a. With the elevation of the master event, NKT2 (1,498 m), and the inverted relative elevations, the elevations of NKT3, NKT4, NKT5, and NKT6 were obtained as 1418 ± 43 , 1639 ± 48 , 1653 ± 47 , and 1604 ± 57 m, respectively. The root mean square (rms) residual will decrease in a straight line (Figure 6a) when one of the relative elevations converges to the optimum and the iteration continues, which can clearly indicate an optimal solution. The relative burial depths of the NKTS nuclear tests were computed as 330, 540 (master event), 506, 468, 521, and 570 m (Table 2). To demonstrate the relationship among the relative burial depths, we projected the source depths and topography onto a profile passing through all six events (zigzagging dashed line in Figure 5), as shown in Figure 6b.

It should be noted that the above results were obtained using a two-step inversion. To validate this approach, we also conducted a one-step joint inversion, and the two sets of results are compared in Table S3. The relative epicenters and elevations from the joint inversion were slightly changed compared to those from the two-step inversion. The joint inversion can simultaneously optimize both objective functions (7) and (8), resulting in smaller standard deviations than those obtained by the two-step method. However, the two-step inversion can avoid a potential trade-off between the depth and origin time. Since the two sets of results are very close, only the two-step results were used in the following yield estimations.

4. Magnitude and Yield Estimates

As one of the basic parameters for a seismic event, the magnitude is generally used to estimate the explosive yield. For a small event such as nuclear explosions at the NKTS, it is easier to obtain high signal-to-noise ratio (SNR) data from regional networks and then calculate the Lg-wave magnitude $m_b(Lg)$ than it is to calculate the teleseismic data-based body-wave magnitude $m_b(P)$. The empirical $m_b(Lg)$ -yield equation by Nuttli (Nuttli, 1973, 1986) is expressed as

$$m_b(Lg) = 5.0 + \log_{10} [A(10) / C], \quad (13)$$

where $A(10)$ and C are the Lg-wave amplitudes generated by the event under investigation and a $m_b = 5$ event at a reference epicentral distance of 10 km. Using World-wide Standardized Seismograph Network (WWSSN) short-period vertical component seismograms, Nuttli (1986, 1973) obtained $C = 110 \mu\text{m}$ for the central United States based on the third peak method, while Patton and Schlittenhardt (2005) obtained $C = 90 \mu\text{m}$ in the same region using the rms amplitude. Through statistical calibration in a given area, the regional magnitude $m_b(Lg)$, body-wave magnitude $m_b(P)$ and local magnitude $M_L(P)$ can be mutually converted. In a series of articles, the Lg-wave magnitudes $m_b(Lg)$ for NKT1-6 were calculated as 3.93, 4.53, 4.91,

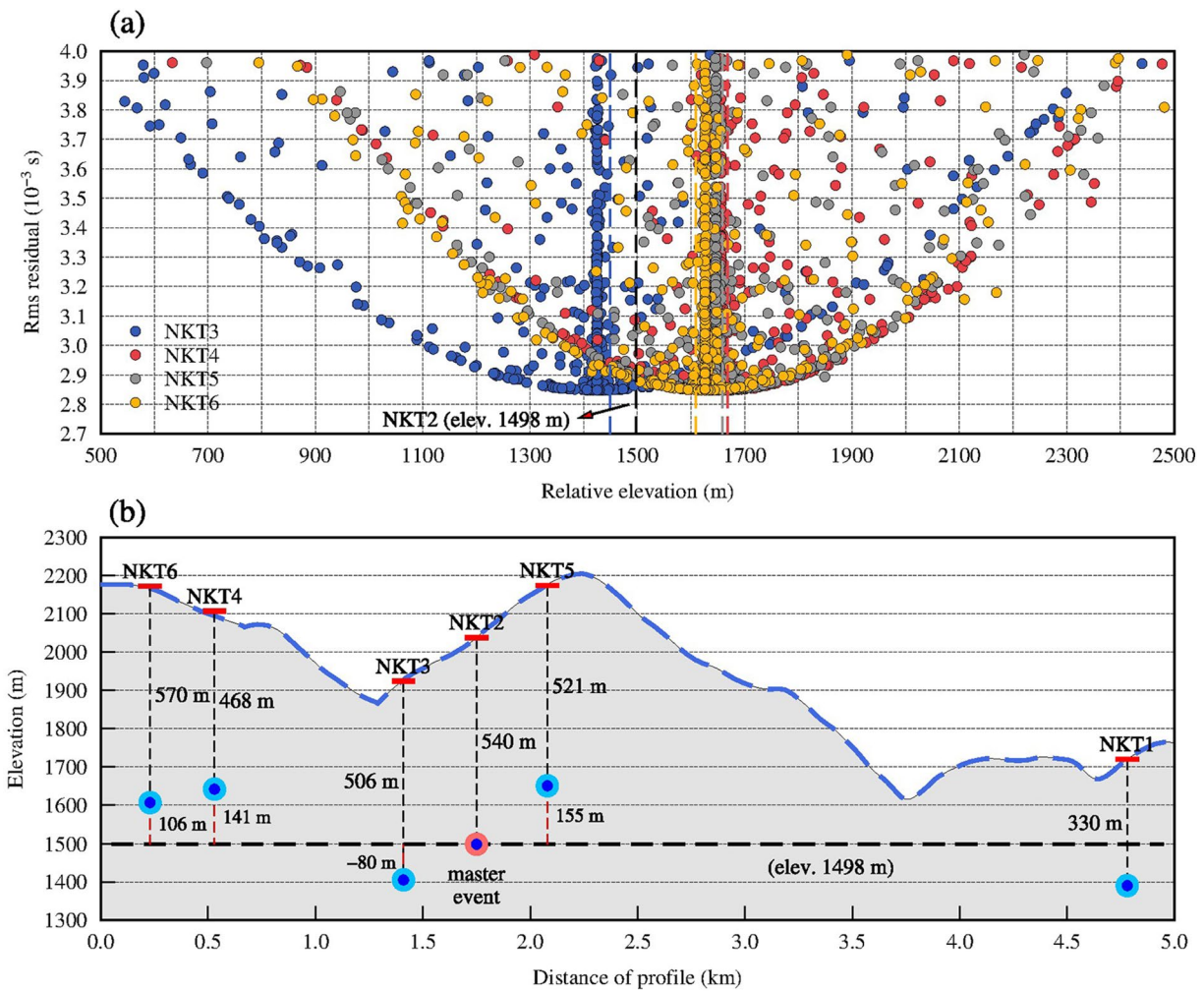


Figure 6. The burial depths along a zigzag profile (dashed line in Figure 5). (a) Convergence of the root mean square (rms) residuals of the relative elevations during the inversion. The relative elevations of NKT3, NKT4, NKT5, and NKT6 rapidly converged to 1418 ± 43 , 1639 ± 48 , 1653 ± 47 and 1604 ± 57 m, respectively, with respect to the master event, NKT2 (1,498 m). Dashed lines with decreasing residuals are shown when a relative elevation converges. (b) Burial depths of the North Korean nuclear tests. The burial depths of NKT1 (330 m) and NKT2 (540 m) were estimated by assuming the elevations of the tunnel entrances, and that of NKT2 was used as the reference depth. The burial depths of NKT3-6 were obtained from the inverted relative elevations, topography and elevation of the master event.

4.67, 4.82, and 5.56 (Xie & Zhao, 2018) using Lg-wave data, broadband Lg-wave attenuation models (Zhao et al., 2010, 2013), and Lg-wave geometric spreading (Yang, 2002). Table 2 lists the regional Lg-wave magnitudes and the teleseismic body-wave magnitudes of the six NKTS explosions given by the USGS National Earthquake Information Center (NEIC) and the Comprehensive Test Ban Treaty Organization (CTBTO).

Several existing empirical magnitude-yield relations may be used to estimate the yields of underground nuclear explosions from their body-wave magnitudes (Bowers et al., 2001; Murphy, 1996; Nuttli, 1986; Ringdal et al., 1992; Zhang & Wen, 2013; Zhao et al., 2008, 2012) or surface wave magnitudes (e.g., Patton, 2016; Stevens & Murphy, 2001). Since the NKTS is an uncalibrated site, we need to estimate the yields of the NKTS tests based on empirical equations from other test sites; among these equations, the empirical magnitude-yield relations from the Nevada test site (Nuttli, 1986), East Kazakhstan (Murphy, 1996; Ringdal et al., 1992) and Novaya Zemlya (Bowers et al., 2001) are shown in Figure 7a, where the solid lines show the parts supported by the observed data and the dashed lines are extrapolations toward smaller magnitudes.

The NKTS at Punggye-ri is located on Mount Mantap, which is characterized by Mesozoic or Jurassic granitic basement rock overlain by a basalt cap (Coblentz & Pabian, 2015). Lg-wave attenuation tomography

Table 2
Best-Fit Burial Depths and Estimated Yields for the North Korean Nuclear Tests

Event code	Date (yyyy/mm/dd)	Elevation ^a (m)	Burial depth ^b (m)	Standard deviation of relative elevation (m)	$m_b(Lg)^d$	Yield ^e (kt)	$m_b(P)^f$ (CTBTO)	Yield (kt)	$m_b(P)^g$ (NEIC)	Yield (kt)
NKT1	2006/10/09	1390 ^c	330	—	3.93	1.0	4.1	1.6	4.3	2.5
NKT2	2009/05/25	1498 ^c	540	Master event	4.53	6.1	4.5	5.7	4.7	9.0
NKT3	2013/02/12	1,418	506	43	4.91	13.7	4.9	13.4	5.1	21.6
NKT4	2016/01/06	1,639	468	48	4.67	7.5	4.9	12.6	5.1	19.8
NKT5	2016/09/09	1,653	521	47	4.82	11.5	5.1	21.7	5.3	34.2
NKT6	2017/09/03	1,604	570	57	5.56	66.1	6.1	225.7	6.3	353.2
Chemical Explosion 1 ^h	1998/08/12	—	7	—	1.94	1.5 (ton)	—	—	—	—
Chemical Explosion 2 ^h	1998/08/18	—	11	—	2.17	1.8 (ton)	—	—	—	—
Chemical Explosion 3 ^h	1998/08/19	—	29	—	2.03	1.45 (ton)	—	—	—	—

^athe elevations extended from the master event using the relative location results. ^bthe burial depths of nuclear tests considering surface elevation differences from the master event (the surface elevations of NKT1-6 are successively 1,720, 2,038, 1,924, 2,107, 2,174, and 2,174 m). ^cthe elevations of NKT1 and NKT2 are based on the elevation differences between the explosion cavities and associated tunnel entrances by assuming a 4% tunnel slope. ^dfrom Xie and Zhao (2018). ^ethe yields of NKT1-6 adjusted by burial depths based on the empirical formula of Bowers et al. (2001). ^ffrom the Comprehensive Test Ban Treaty Organization (CTBTO). ^gfrom the USGS National Earthquake Information Center (NEIC). ^hthe source parameters of three chemical explosions provided by the Geophysical Exploration Center of the China Earthquake Administration (GECCEA).

(Zhao et al., 2013) revealed that the crust in North Korea has a significantly high Q value, which suggests that the NKTS is in a stable region with a relatively hard crust. This is clearly different from the situation at the American Nevada test site, which is characterized by relatively weak tuff and rhyolite. Therefore, compared with the empirical equation by Nuttli (1986) based on data from the Nevada test site, the empirical formula of Bowers et al. (2001) based on data from a region with a stable shield structure should be more suitable for the NKTS:

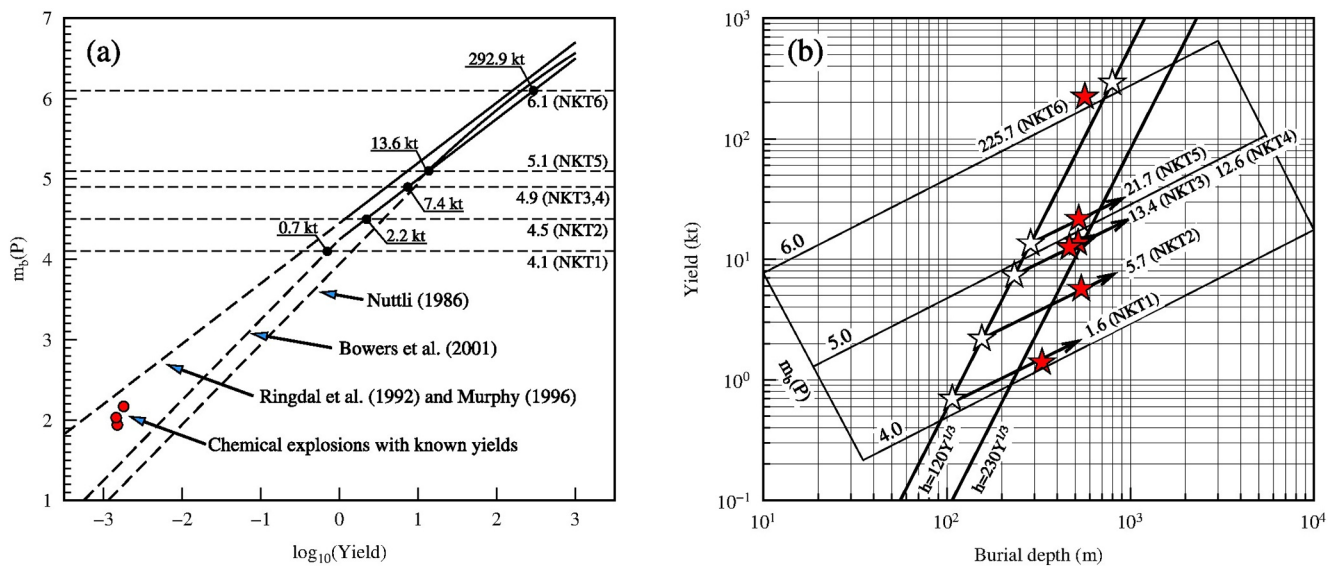


Figure 7. Yield estimates based on empirical magnitude-yield relations. (a) Three magnitude-yield empirical relations at the Nevada test site (Nuttli, 1986), East Kazakhstan (Murphy, 1996; Ringdal et al., 1992) and Novaya Zemlya (Bowers et al., 2001). The solid lines show the parts supported by data, and the dashed lines are extrapolations to smaller magnitudes. By assuming normally scaled burial depths, the yields of NKT1-6 estimated using the empirical equation of Bowers et al. (2001) are illustrated. The red solid circles represent three small chemical explosions with known source parameters. (b) Yield estimates for NKT1-6 without (open stars) and with (red stars) burial depth corrections. The normally scaled depth $h = 120Y^{1/3}$ and another overburied scaled depth $h = 230Y^{1/3}$ are included for reference.

$$m_b = 4.25 + \beta \log Y, \quad (14)$$

where m_b is the body-wave magnitude, Y is the yield in kt, and β is 0.75 for $Y \geq 1$ kt and 1.0 for $Y < 1$ kt. In addition, the magnitudes and yields of three chemical explosions (red solid circles in Figure 7a) with known source parameters (listed in Table 2) provided by the Geophysical Exploration Center of the China Earthquake Administration (GECCEA) are close to those from the empirical formula of Bowers et al. (2001) at the low-magnitude end. Implicitly, this empirical relation is intended for fully coupled explosions at normally scaled burial depths ($h = 120Y^{1/3}$). Therefore, to extend the above empirical relation to events that deviate from a normally scaled burial depth, Patton and Taylor (2011) proposed a depth correction term:

$$-0.7875 \cdot \log \left[h / \left(120Y^{1/3} \right) \right], \quad (15)$$

where h is the burial depth (m).

We used the magnitude-yield Equation 14, the depth correction (Equation 15), and the burial depths obtained in this study to estimate the yields of the six NKTS nuclear explosions from body-wave magnitudes m_b , including the regional magnitude $m_b(Lg)$ calculated using Equation 13 and the teleseismic P -wave magnitude $m_b(P)$ from the CTBTO and USGS. The yields with depth corrections are listed in Table 2. The $m_b(P)$ values of the six NKTS explosions provided by the USGS and CTBTO are systematically higher than the $m_b(Lg)$ values from this study; this deviation between $m_b(P)$ and $m_b(Lg)$ may be because the former was measured from P waves while the latter was measured from S waves, and the P/S amplitude ratio varies with the source type (earthquake vs. explosion), frequency, and magnitude (Ma et al., 2021). This is also part of the reason why P/S spectral ratios can be leveraged to distinguish explosions and earthquakes (e.g., Taylor et al., 1989; Zhao et al., 2014). Consequently, the yields calculated by $m_b(Lg)$ may be underestimated. Figure 7b illustrates the changes in the yields estimated from the CTBTO $m_b(P)$ before (open stars) and after (red stars) applying the depth correction. These results demonstrate that the NKT1-5 were likely overburied and close to a scaled depth of $h = 230Y^{1/3}$, although NKT6 was close to the normally scaled depth.

5. Discussion

5.1. Accuracy and Robustness of the Proposed Relocation Method

The obtained relative epicenters using both Pg and Pn data are consistent with those of previous studies using Pn or teleseismic P waves (e.g., Gibbons et al., 2017; He et al., 2018; Wei, 2017; Myers et al., 2018). Compared with the epicenters reported by He et al. (2018) using Pn waveform data, our epicenters of NKT4 and NKT6 are shifted approximately 200 and 350 m toward the east, which are closer to the absolute epicenters obtained from surface damage (Figure 5), and there are minor changes in the relative epicenters of NKT3 and NKT5. These deviations may be attributed to the burial depths or uncertainties in the Pn and Pg velocities. Comparing the NKTS epicenters announced by the North Korean military with those obtained by us and by He et al. (2018) (Figure 5) reveals that the locations obtained in this study are closer to those from the North Korean military, and the differences can be attributed largely to the location of the master event. In contrast, the epicenters obtained by previous seismic methods or InSAR data are all shifted to the west slope of Mount Mantap (Gibbons et al., 2017; He et al., 2018; Wei, 2017; Myers et al., 2018; Sreejith et al., 2020). The results using the military location of NKT2 as the master event are shown in Figure 8f, indicating that the two groups of epicenters are highly consistent.

In traditional depth location methods, the traveltimes-determined focal depth is accurate only when the epicentral distance is less than 1.4 times the focal depth (Mori, 1991). For sources with very shallow depths, such as the North Korean nuclear explosions, the traveltimes are generally considered to provide a poor constraint on the burial depth (Pasyanos & Myers, 2018). Therefore, the depth phases such as the pP waves were often used to provide additional constraints, either explicitly or implicitly. Murphy et al. (2013) used the teleseismic P -wave spectral ratio method to estimate the optimal depths of NKT1 and NKT2 as 200 and 550 m, respectively, and used the depths with minimum traveltimes residuals as independent evidence to support their results. Rougier et al. (2011) inverted a minimum depth of 375 m for NKT2 by using the hydro-

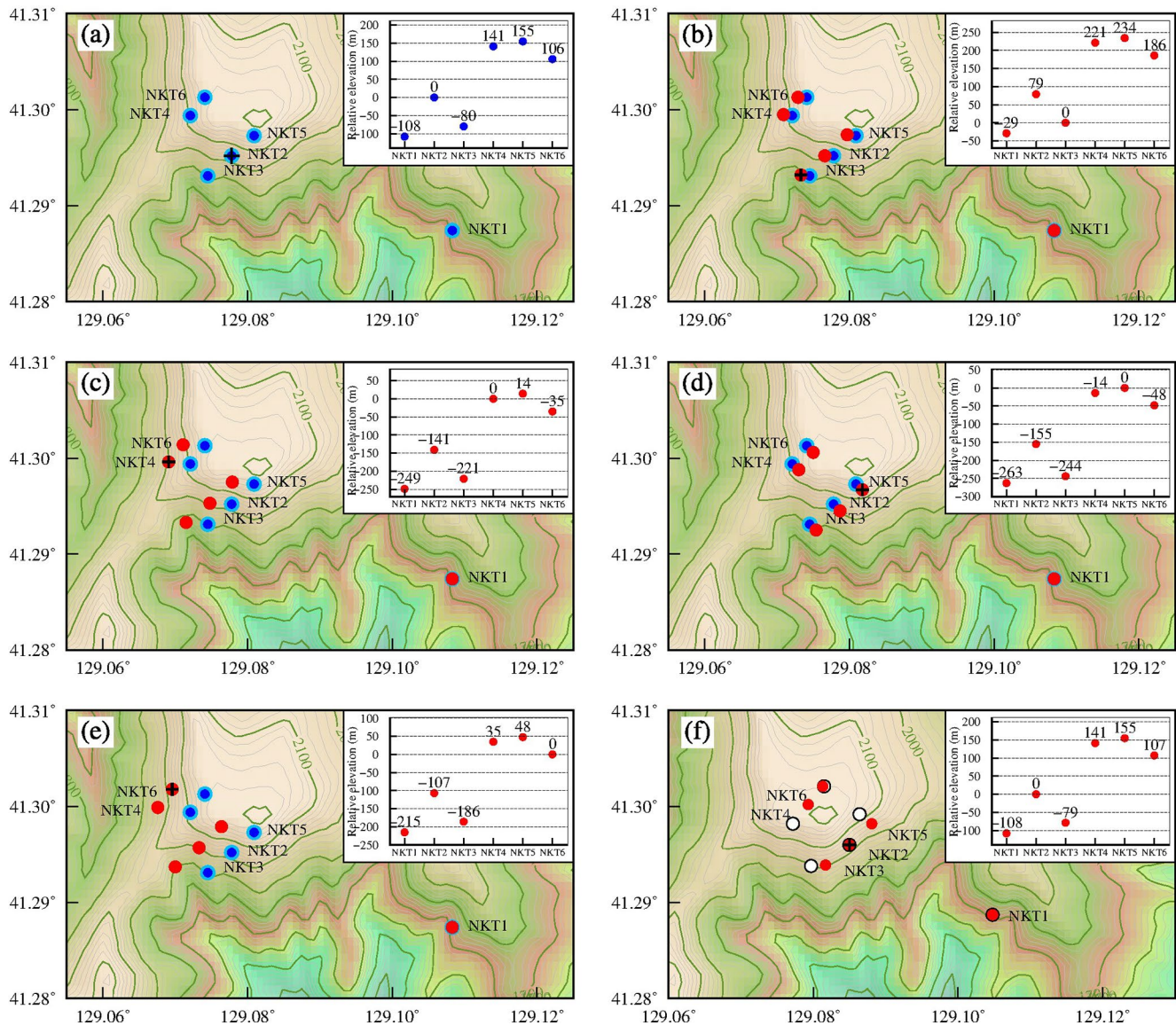


Figure 8. Relative epicenters and elevations of NKT1-6 obtained using different master events. (a) Relative epicenters (blue solid circles) and elevations using NKT2 as the master event. (b-e) Relative epicenters (red solid circles) and elevations if using the epicenters of NKT3, NKT4, NKT5, or NKT6 reported by He et al. (2018) as the master event (marked with crosses). The elevation differences relative to different master events (0 m) are displayed in the inset figures. (f) Relative epicenters (red solid circles) and elevations using the military-provided NKT2 epicenter as the master event, with other epicenters from the military shown in white solid circles for comparison.

dynamic calculation method. Some previous estimates of the burial depths of the six underground nuclear tests are listed in Table 3. One common feature among these methods is that the yield and burial depth are inverted simultaneously. Although these techniques can limit the fitting errors to an acceptable level, the result may deviate from the actual depth if the trade-off between the yield and burial depth is not completely resolved (Koper et al., 2008). Using the regional envelope method based on the preferred Walter-Ford explosion source model, Pasyanos and Myers (2018) estimated that the burial depths and yields of NKT1-6 were 421 m/1.7 kt, 447 m/8.0 kt, 390 m/16.0 kt, 592 m/13.5 kt, 568 m/41.0 kt, and 636 m/149.0 kt. In their study, in addition to the seismic data, the burial depths were further constrained by the locations of tunnel entrances, tunnel slopes and local topographies near the explosion cavities (Pasyanos & Myers, 2018). More recently, Voytan et al. (2019) used high-frequency teleseismic *P*-wave amplitude modeling and waveform equalization to estimate the yields of the six NKTs tests; the resulting burial depths were specified as 430, 600, 430, 710, 710, and 710 m in chronological order based on the assumption of a 4% tunnel slope to meet

Table 3
Comparison of the Burial Depths (m) of the North Korean Nuclear Tests From Different Studies

2006/10/09	2009/05/25	2013/02/12	2016/01/06	2016/09/09	2017/09/03	Data type	References
200	550					Pn spectral ratio	Murphy et al. (2010)
	375					Hydrodynamic calculation	Rougier et al. (2011)
		610	430			Tunnel entrance/site elev.	Zhang & Wen (2013)
			420–700			Surface damage from InSAR	Wei (2017)
					760	Tunnel entrance/site elev.	Tian et al. (2018)
					450 ± 100	Surface damage from InSAR	Wang et al. (2018)
			760			Surface damage from InSAR	Myers et al. (2018)
421	447	390	592	568	636	Wave envelope/W-F source	Pasyanos & Myers (2018)
430	600	430	710	710	710	Tunnel entrance/site elev.	Voytan et al. (2019)
					542 ± 30	Surface damage from InSAR	Sreejith et al. (2020)
330	540	506	468	521	570	Pn and Pg waveforms	This study

Abbreviation: InSAR, interferometric synthetic aperture radar.

drainage requirements (Sinha, 1991). Similar estimates of burial depths were also used in other studies (Tian et al., 2018; Zhang & Wen, 2013). However, these burial depth estimates are based largely on epicenter locations and assumptions regarding the tunnel geometry. Another non-seismic information, satellite images of the surface displacements caused by relatively shallow explosions can provide independent evidence for epicenter and burial depth (Schlittenhardt et al., 2010; Sreejith et al., 2020; Wang et al., 2018) but are less sensitive for overburied events. Although the burial depths in this study are still affected by the surface elevations above the sources and the elevation of the master event, the relative elevations of these events are determined solely based on seismic data by combining both Pn and Pg phases. The burial depths of NKT1-6 are all within the 300–600 m range, which are consistent with the depths reported in previous studies (Wei, 2017; Murphy et al., 2010; Pasyanos & Myers, 2018; Rougier et al., 2011; Sreejith et al., 2020; Tian et al., 2018; Wang et al., 2018; Zhang & Wen, 2013). The Pn and Pg phases can be easily identified and readily available in regional seismic data, making this method very attractive for quickly locating the epicenter and depth of a potential nuclear test at a known test site.

To illustrate the accuracy and robustness of the proposed depth location method, we investigated the influence of using different master events in the two-step inversion. In this study, NKT2 was used as the master event. We tested utilizing the NKT3, NKT4, NKT5, and NKT6 reported by He et al. (2018), as well as that of NKT2 provided by the North Korean military, as the master events, and the resulting epicenters and elevation differences are shown in Figure 8. The absolute epicenters of NKT2-6 changed with the changing of the master event, but the relative elevations remained almost unchanged because of the consistent relative epicenter locations.

In addition, we also tested the impacts of different velocity models on the relative epicenters and elevations. As an example, we used the IASP91 Reference Earth Model (Kennett et al., 1995) and NKT2 as the master event to determine the relative locations, and the results are illustrated in Figure 9. In this example, the relative epicenters are slightly changed, and the relative elevations are changed by only 20–40 m, which is because IASP91 has a slightly higher (5.8 km/s) near-surface *P*-wave velocity than the Korean velocity model (Bonner et al., 2008; Herrmann et al., 2005) used here. In summary, the current method is robust for using different master events or velocity models.

5.2. Uncertainties in the Relative Epicenter, Burial Depth, and Yield Estimates

Tables 1 and 2 list the uncertainties in the relative epicenters and standard deviations of the relative elevations calculated by randomly selecting 80% of the data in each inversion (Efron, 1983), which indicate that the uncertainties of relative locations based on the proposed method and used regional data set are very small. However, the inversion process is based on simple approximations such as the locally flat Moho

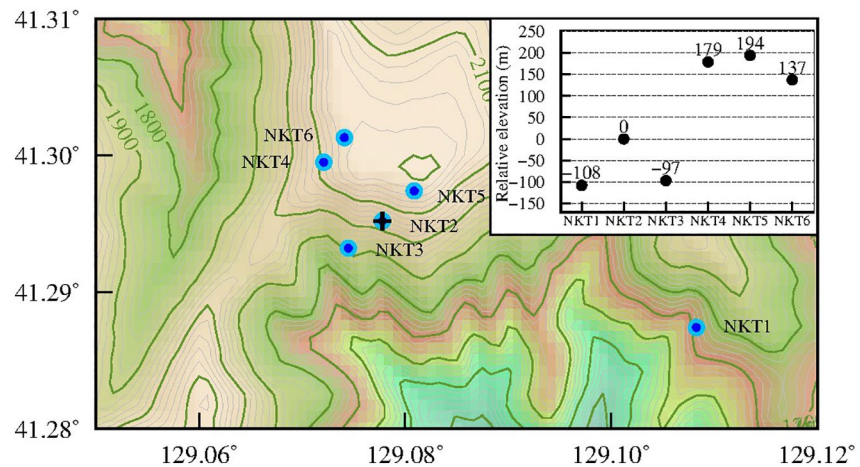


Figure 9. Similar to Figure 8a except the crust and upper mantle velocities are from the IASP91 Reference Earth Model.

discontinuity and topography, and simple near source velocity model, and so on, while the anisotropic property of sources, complexity of the Pg waves (scattering from both the free surface and local heterogeneities, multi-pathing), coupled sensitivities of Pg and Pn waves to depth and epicenters, can all add errors to the results. Furthermore, as already discussed above, to convert the relative epicenters and source elevations to the absolute epicenters and burial depths, additional factors, such as the location of the master event, the local 3D velocity and topography are all involved. Without the ground truth information, the actual uncertainties of the epicenters and focal depth are difficult to quantify. Therefore, we should understand the actual uncertainties could be well larger than the nominal uncertainties of relative location.

In this study, we re-estimated the yields of NKT1-6 by first using an empirical yield-magnitude relation (Bowers et al., 2001; Patton & Taylor, 2011) to obtain their yields assuming normally scaled depths, followed by a depth correction using the equation by Patton and Taylor (2011). Based on the CTBTO body wave magnitudes $m_b(P)$ and the relocated depths from this study, the re-estimated yields in Table 2 are consistent with those reported in previous studies (e.g., Sreejith et al., 2020; Voytan et al., 2019). In using the depth correction Equation 15, a 100-m uncertainty in the absolute depth, can cause a variation of approximately 13%–24% in the NKT yield estimate. However, determining the yield of a nuclear test at an uncalibrated test site is still a challenge. The body-wave magnitude $m_b(P)$ is the basic parameter in estimating the explosive yield, but the teleseismic P -wave signals produced by small North Korean nuclear tests and recorded at global networks are of relatively poor quality, which may greatly increase the uncertainties in the yield estimates. On the other hand, using the body wave magnitude based on the regional Lg-wave, although with a high SNR, often underestimates the yields of nuclear explosions. We must consider whether it is appropriate to apply an empirical relation based on one test site to other, as-of-yet uncalibrated sites or whether it is feasible to extend an empirical equation calibrated with larger-yield events to smaller-yield events. Hence, it will be difficult to solve without the ground true information.

5.3. Possible Burial Methods

To determine the burial depths of NKT1 and NKT2, we assumed that the tunnel entrances are connected to the explosions by straight tunnels with a 4% slope. However, from an engineering perspective, tunnels are likely to be designed according to older design schemes from Pakistan or the United States, namely, as a longer zigzag tunnel and a fish hook-shaped tunnel near the explosion cavity to assist with “self-sealing” after detonation. The possible burial methods and three-dimensional models of tunnels for the NKTS tests are shown in Figure 10. NKT1 and NKT2 are connected to the east entrance and west entrance, respectively, by two long zigzag tunnels. The east tunnel was obviously abandoned after NKT1 in 2006, whereas the tunnel connected to NKT2 was used many times in subsequent nuclear tests (Figure 10a). Downward and upward shafts near NKT3 and NKT4-6, respectively, are relatively acceptable for satisfying the different

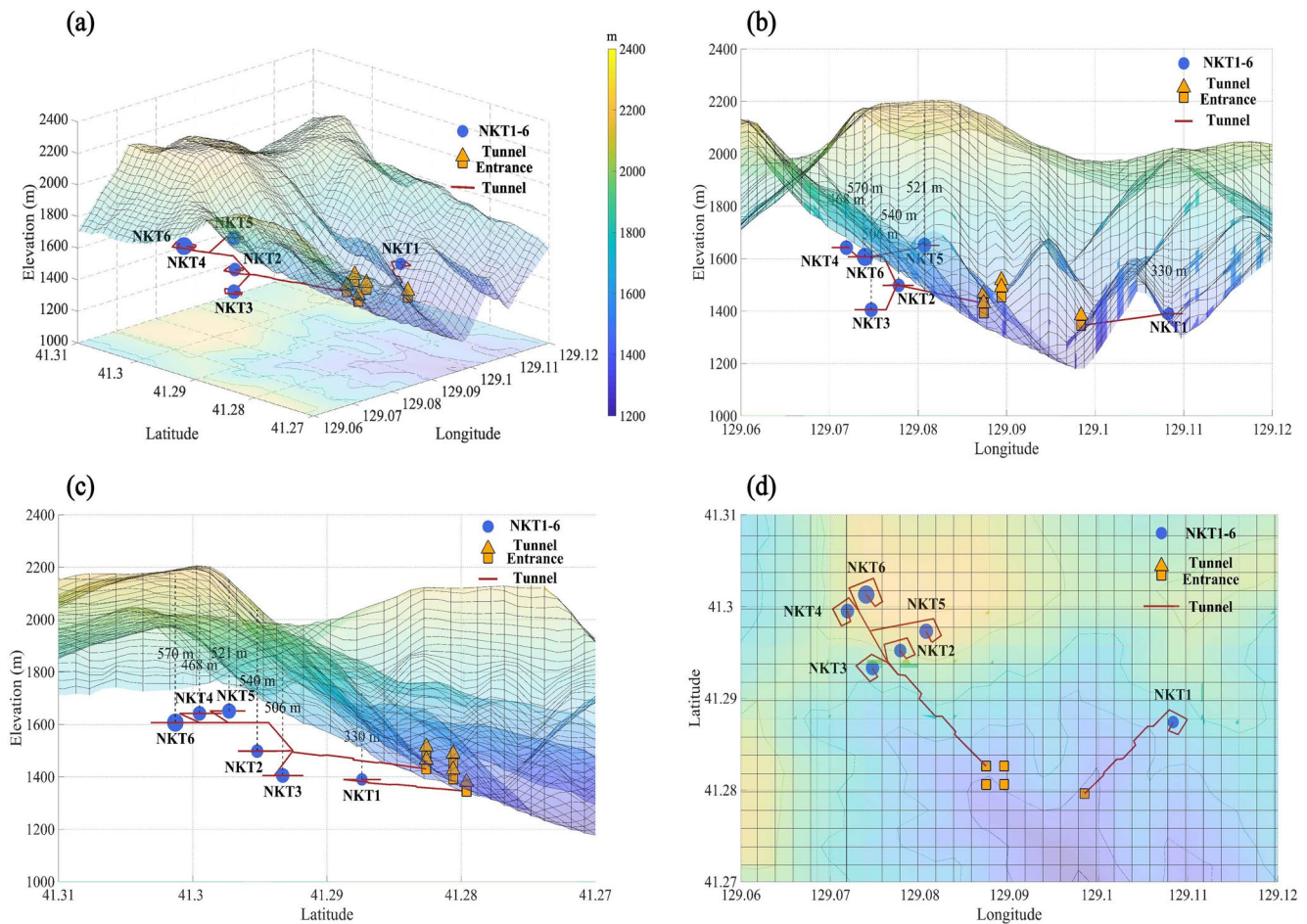


Figure 10. Possible burial methods of the North Korean nuclear tests. (a–d) Panoramic, front, lateral and vertical views of the possible burial methods of the North Korean nuclear tests. NKT1 and NKT2 are connected to the east entrance and west entrance, respectively, by zigzag tunnels with a 4% slope to meet the drainage requirements (Sinha, 1991), and there are some fish hook-shaped tunnels near the explosion cavities to assist with “self-sealing” after detonation. There may be a downward shaft in the tunnel connected to NKT3, and a model with a common upward shaft near the explosion cavities is more acceptable for the last three NKTS nuclear tests.

relative elevation requirements speculated in this study (Figures 10b and 10c) and are likely to prevent repeated contamination by radionuclides. Interestingly, NKT1-3 have similar elevations, and the elevations of the three recent nuclear experiments are also very close, indicating that they likely shared a common tunnel shaft. Similar burial methods for NKT4-6 coincidentally correspond well with the origin times, which may indicate that the three consecutive nuclear experiments between January 2016 and September 2017 were carried out at virtually identical elevations to accelerate the nuclear experiments and reduce development costs. However, these tunnel models are only rough estimates based on the locations of the nuclear tests and tunnel entrances, and many speculations about the construction of these tunnels need further proof.

6. Conclusions

A high-precision relative location method based on Pn and Pg phases was proposed to relocate epicenters and focal depths of a group of adjacent seismic events such as the North Korean nuclear tests. The Pn and Pg signals have quite different takeoff angles. Combining both phases together can reasonably balance the trade-off between the burial depth and origin time. The North Korean nuclear tests produced abundant regional waveforms. Due to their very closed source locations and nearly identical mechanisms, these waveforms have excellent cross-correlations with each other when recorded at the same station. The resulted DTTs provided highly accurate relative epicenters and relative depths. Our estimated burial depths

for the six North Korean nuclear tests are in the range of 300–600 m and these depths can further improve the yield estimates. Based on a relocated burial depth of 570 m, the yield for the largest nuclear explosion at the NKTS is approximately 225.7 kt after the depth correction. Due to very closed source locations, highly consistent source mechanisms and a large high quality broadband regional seismic data set, the relative relocation procedural has very small uncertainties, although the actual uncertainties of absolute locations could be larger owing to many other factors such as the information of the master event.

Data Availability Statement

The waveforms recorded at the CNDSN, GSN, and F-net stations used in this study were collected from the China Earthquake Networks Center (CENC), the Data Management Centre of the China National Seismic Network at the Institute of Geophysics, China Earthquake Administration (SEIDMC; Zheng et al., 2010) at <http://www.seidmc.ac.cn> (last accessed April 2020), the Incorporated Research Institutions for Seismology Data Management Center (IRIS-DMC) at www.iris.edu (last accessed April 2020), and the National Research Institute for Earth Science and Disaster Prevention (NIED) at <http://www.fnet.bosai.go.jp> (last accessed April 2020). The tunnel construction photo published on North Korean television and some information about the nuclear test tunnels are from <https://www.38north.org/2018/05/punggyetunnel052318/>, where some photos were obtained from the National Nuclear Security Administration (<https://www.energy.gov/nnsa/national-nuclear-security-administration>). Certain figures were generated using Generic Mapping Tools (GMT; Wessel & Smith, 1998).

Acknowledgments

The comments from Editor Yehuda Ben-Zion, the associate editor and two anonymous reviewers are valuable and greatly improved this manuscript. This research was supported by the National Key Research and Development Program of China (2017YFC0601206), the National Natural Science Foundation of China (41674060, 41630210, 41974054, and 41974061), and the Special Fund of China Seismic Experimental Site (2019CSES0103, 2016CSES0203).

References

- Bonner, J., Herrmann, R. B., Harkrider, D., & Pasyanos, M. (2008). The surface wave magnitude for the 9 October 2006 North Korean nuclear explosion. *Bulletin of the Seismological Society of America*, 98(5), 2498–2506. <https://doi.org/10.1785/0120080929>
- Bowers, D., Marshall, P. D., & Douglas, A. (2001). The level of deterrence provided by data from the SPITS seismometer array to possible violations of the Comprehensive Test Ban in the Novaya Zemlya region. *Geophysical Journal International*, 146, 425–438. <https://doi.org/10.1046/j.1365-246x.2001.01462.x>
- Campillo, M., Bouchon, M., & Massinon, B. (1984). Theoretical study of the excitation, spectral characteristics, and geometrical attenuation of regional seismic phases. *Bulletin of the Seismological Society of America*, 74, 79–90.
- Coblentz, D., & Pabian, F. (2015). Revised geologic site characterization of the North Korean test site at Punggye-ri. *Science and Global Security*, 23(2), 101–120. <https://doi.org/10.1080/08929882.2015.1039343>
- Efron, B. (1983). Estimating the error rate of a prediction rule: Improvement on cross-validation. *Journal of the American Statistical Association*, 78, 316–331. <https://doi.org/10.2307/2288636>
- Gibbons, S. J., Pabian, F., Näsholm, S. P., Kväerna, T., & Mykkeltveit, S. (2017). Accurate relative location estimates for the North Korean nuclear tests using empirical slowness corrections. *Geophysical Journal International*, 208(1), 101–117. <https://doi.org/10.1093/gji/ggw379>
- Greensfelder, R. W. (1965). The Pg-Pn method of determining depth of focus with applications to Nevada earthquakes. *Bulletin of the Seismological Society of America*, 55(2), 391–403.
- He, X., Zhao, L. F., Xie, X. B., & Yao, Z. X. (2018). High-precision relocation and event discrimination for the 3 September 2017 underground nuclear explosion and subsequent seismic events at the North Korean test site. *Seismological Research Letters*, 89(6), 2042–2048. <https://doi.org/10.1785/0220180164>
- Herrmann, R. B., Jeon, Y. S., & Yoo, H. J. (2005). *Proceedings of the 4th International Seminar on Seismic Tomography of Far-East Asia and Related words*. Korea Institute of Geoscience and Mineral Resources.
- Kennett, B. L. N., Engdahl, E. R., & Buland, R. (1995). Constraints on seismic velocities in the Earth from traveltimes. *Geophysical Journal International*, 122, 108–124. <https://doi.org/10.1111/j.1365-246X.1995.tb03540.x>
- Kirkpatrick, S., Gelatt, C. D., & Vecchi, M. P. (1983). Optimization by simulated annealing. *Science*, 220, 671–680. <https://doi.org/10.1126/science.220.4598.671>
- Koper, K. D., Herrmann, R. B., & Benz, H. M. (2008). Overview of open seismic data from the North Korean event of 9 October 2006. *Seismological Research Letters*, 79(2), 178–185. <https://doi.org/10.1785/gssrl.79.2.178>
- Ma, X., Zhao, L. F., Xie, X. B., He, X., & Yao, Z. X. (2021). Regional seismic characteristics of chemical explosions on the eastern margin of the Junggar Basin, Northwest China, and of historical Semipalatinsk nuclear tests. *Bulletin of the Seismological Society of America*, 111(1), 606–620. <https://doi.org/10.1785/0120200151>
- Mori, J. (1991). Estimates of velocity structure and source depth using multiple P waves from aftershocks of the 1987 Elmore Ranch and Superstition Hills, California, earthquakes. *Bulletin of the Seismological Society of America*, 81(2), 508–523.
- Murphy, J. R. (1996). Type of seismic events and their source descriptions. In E. S. Husebye, & A. M. Dainty (Eds.), *Monitoring a comprehensive Test Ban Treaty* (pp. 225–245). Kluwer Academic Publishers. https://doi.org/10.1007/978-94-011-0419-7_16
- Murphy, J. R., Stevens, J. L., Kohl, B. C., & Bennett, T. J. (2013). Advanced seismic analyses of the source characteristics of the 2006 and 2009 North Korean nuclear tests. *Bulletin of the Seismological Society of America*, 103(3), 1640–1661. <https://doi.org/10.1785/0120120194>
- Murphy, R. J., Kohl, B. C., Stevens, J. L., Bennett, T. J., & Israelsson, H. G. (2010). Exploitation of the IMS and other data for a comprehensive, advanced analysis of the North Korean nuclear tests. In *Monitoring Research Review: Ground-Based Nuclear Explosion Monitoring Technologies LA-UR-10-05578* (pp. 456–465).
- Myers, S. C., Ford, S. R., Mellors, R. J., Baker, S., & Ichinose, G. (2018). Absolute locations of the North Korean nuclear tests based on differential seismic arrival times and InSAR. *Seismological Research Letters*, 89(6), 2049–2058. <https://doi.org/10.1785/0220180123>

- Nuttli, O. W. (1973). Seismic wave attenuation and magnitude relations for eastern North America. *Journal of Geophysical Research*, 78(5), 876–885. <https://doi.org/10.1029/JB078i005p00876>
- Nuttli, O. W. (1986). Yield estimates of Nevada test site explosions obtained from seismic Lg waves. *Journal of Geophysical Research*, 91(B2). <https://doi.org/10.1029/JB091iB02p02137>
- Pasyanos, M. E., & Ford, S. R. (2015). Determining the source characteristics of explosions near the Earth's surface. *Geophysical Research Letters*, 42(10), 3786–3792. <https://doi.org/10.1002/2015gl063624>
- Pasyanos, M. E., & Myers, S. C. (2018). The coupled location/depth/yield problem for North Korea's declared nuclear tests. *Seismological Research Letters*, 89(6), 2059–2067. <https://doi.org/10.1785/0220180109>
- Pasyanos, M. E., Walter, W. R., & Mayeda, K. M. (2012). Exploiting regional amplitude envelopes: A case study for earthquakes and explosions in the Korean Peninsula. *Bulletin of the Seismological Society of America*, 102(5), 1938–1948. <https://doi.org/10.1785/0120120012>
- Patton, H. J. (2016). A physical basis for Ms-yield scaling in hard rock and implications for late-time damage of the source medium. *Geophysical Journal International*, 206(1), 191–204. <https://doi.org/10.1093/gji/ggw140>
- Patton, H. J., & Schlittenhardt, J. (2005). A transportable scale for central Europe and implications for low-magnitude discrimination. *Geophysical Journal International*, 163(1), 126–140. <https://doi.org/10.1111/j.1365-246X.2005.02663.x>
- Patton, H. J., & Taylor, S. R. (2011). The apparent explosion moment: Inferences of volumetric moment due to source medium damage by underground nuclear explosions. *Journal of Geophysical Research*, 116(B3), B03310. <https://doi.org/10.1029/2010JB007937>
- Ringdal, F., Marshall, P. D., & Alewine, R. W. (1992). Seismic yield determination of Soviet underground nuclear explosions at the Shagan River test site. *Geophysical Journal International*, 109, 65–77. <https://doi.org/10.1111/j.1365-246X.1992.tb00079.x>
- Rougier, E., Patton, H. J., Knight, E. E., & Bradley, C. R. (2011). Constraints on burial depth and yield of the 25 May 2009 North Korean test from hydrodynamic simulations in a granite medium. *Geophysical Research Letters*, 38(16), L16316. <https://doi.org/10.1029/2011gl048269>
- Sato, H., & Fehler, M. C. (1998). *Seismic wave propagation and scattering in the heterogeneous Earth*. Springer Berlin Heidelberg.
- Schaff, D. P., Kim, W. Y., Richards, P. G., Jo, E., & Ryoo, Y. (2018). Using waveform cross correlation for detection, location, and identification of aftershocks of the 2017 nuclear explosion at the North Korea test site. *Seismological Research Letters*, 89, 6. <https://doi.org/10.1785/0220180132>
- Schaff, D. P., & Richards, P. G. (2004). Repeating seismic events in China. *Science*, 303, 1176–1178. <https://doi.org/10.1126/science.1093422>
- Schlittenhardt, J., Cauty, M., & Grünberg, I. (2010). Satellite earth observations support CTBT monitoring: A case study of the nuclear test in North Korea of Oct. 9, 2006 and comparison with seismic results. *Pure and Applied Geophysics*, 167(4–5), 601–618. <https://doi.org/10.1007/s00024-009-0036-x>
- Selby, N. D. (2010). Relative locations of the October 2006 and May 2009 DPRK announced nuclear tests using international monitoring system seismometer arrays. *Bulletin of the Seismological Society of America*, 100(4), 1779–1784. <https://doi.org/10.1785/0120100006>
- Sinha, R. S. (1991). *Underground Structures: Design and construction*. Elsevier Science Publishing Company.
- Sreejith, K. M., Agrawal, R., & Rajawat, A. S. (2020). Constraints on the location, depth and yield of the 2017 September 3 North Korean nuclear test from InSAR measurements and modeling. *Geophysical Journal International*, 220(1), 345–351. <https://doi.org/10.1093/gji/ggz451>
- Stevens, J. L., & Murphy, J. R. (2001). Yield estimation from surface wave amplitudes. *Pure and Applied Geophysics*, 155(11), 2227–2251. <https://doi.org/10.1007/Pl00001147>
- Taylor, S. R., Denny, M. D., Vergino, E. S., & Glaser, R. E. (1989). Regional discrimination between NTS explosions and western U.S. earthquakes. *Bulletin of the Seismological Society of America*, 79, 1142–1176
- Tian, D. D., Yao, J. Y., & Wen, L. X. (2018). Collapse and earthquake swarm after North Korea's 3 September 2017 nuclear test. *Geophysical Research Letters*, 45(9), 3976–3983. <https://doi.org/10.1029/2018gl077649>
- Tibuleac, I. M., von Seggern, D. H., Anderson, J. G., Smith, K. W., Aburto, A., & Rennie, T. (2008). Location and magnitude estimation of the 9 October 2006 Korean nuclear explosion using the Southern Great Basin Digital Seismic Network as a large-aperture array. *Bulletin of the Seismological Society of America*, 98(2), 756–767. <https://doi.org/10.1785/0120070046>
- Voytan, D. P., Lay, T., Chaves, E. J., & Ohman, J. T. (2019). Yield estimates for the six North Korean nuclear tests from teleseismic P wave modeling and intercorrelation of P and Pn recordings. *Journal of Geophysical Research: Solid Earth*, 124(5), 4916–4939. <https://doi.org/10.1029/2019jb017418>
- Wagner, M., Husen, S., Lomax, A., Kissling, E., & Giardini, D. (2013). High-precision earthquake locations in Switzerland using regional secondary arrivals in a 3-D velocity model. *Geophysical Journal International*, 193(3), 1589–1607. <https://doi.org/10.1093/gji/ggt052>
- Waldhauser, F., & Ellsworth, W. L. (2000). A Double-difference earthquake location algorithm: Method and application to the Northern Hayward Fault, California. *Bulletin of the Seismological Society of America*, 90(6), 1353–1368. <https://doi.org/10.1785/0120000006>
- Wang, T., Shi, Q. B., Nikkhoo, M., Wei, S. J., Barbot, S., Dreger, et al. (2018). The rise, collapse, and compaction of Mt. Mantap from the 3 September 2017 North Korean nuclear test. *Science*, 361, 166–170. <https://doi.org/10.1126/science.aar7230>
- Wei, M. (2017). Location and source characteristics of the 2016 January 6 North Korean nuclear test constrained by InSAR. *Geophysical Journal International*, 209(2), 762–769. <https://doi.org/10.1093/gji/ggx053>
- Wei, X., Wang, X. T., & Li, Z. W. (2019). Initial rupture depth of the 8 August 2017 M7.0 Jiuzhaigou earthquake derived from Pn/Pg relative location. *Chinese Journal of Geophysics*, 62(4), 1300–1311. <https://doi.org/10.6038/cjg2019L0796>
- Wen, L. X., & Long, H. (2010). High-precision location of North Korea's 2009 nuclear test. *Seismological Research Letters*, 81(1), 26–29. <https://doi.org/10.1785/gssrl.81.1.26>
- Wessel, P., & Smith, W. H. F. (1998). New, improved version of generic mapping tools released. *Eos Transactions AGU*, 79, 579. <https://doi.org/10.1029/98eo00426>
- Xie, X. B., & Zhao, L. F. (2018). The seismic characterization of North Korea underground nuclear tests. *Chinese Journal of Geophysics*, 61(3), 889–904. <https://doi.org/10.6038/cjg2018L0677>
- Yang, X. N. (2002). A numerical investigation of Lg geometrical spreading. *Bulletin of the Seismological Society of America*, 92(8), 3067–3079. <https://doi.org/10.1785/0120020046>
- Zhang, M., & Wen, L. X. (2013). High-precision location and yield of North Korea's 2013 nuclear test. *Geophysical Research Letters*, 40(12), 2941–2946. <https://doi.org/10.1002/grl.50607>
- Zhao, L. F., Xie, X. B., Wang, W. M., Fan, N., Zhao, X., & Yao, Z. X. (2017). The 9 September 2016 North Korean underground nuclear test. *Bulletin of the Seismological Society of America*, 107(6), 3044–3051. <https://doi.org/10.1785/0120160355>
- Zhao, L. F., Xie, X. B., Wang, W. M., Hao, J. L., & Yao, Z. X. (2016). Seismological investigation of the 2016 January 6 North Korean underground nuclear test. *Geophysical Journal International*, 206(3), 1487–1491. <https://doi.org/10.1093/gji/ggw239>
- Zhao, L. F., Xie, X. B., Wang, W. M., & Yao, Z. X. (2008). Regional seismic characteristics of the 9 October 2006 North Korean nuclear test. *Bulletin of the Seismological Society of America*, 98(6), 2571–2589. <https://doi.org/10.1785/0120080128>

- Zhao, L. F., Xie, X. B., Wang, W. M., & Yao, Z. X. (2012). Yield estimation of the 25 May 2009 North Korean nuclear explosion. *Bulletin of the Seismological Society of America*, *102*(2), 467–478. <https://doi.org/10.1785/0120110163>
- Zhao, L. F., Xie, X. B., Wang, W. M., & Yao, Z. X. (2014). The 12 February 2013 North Korean underground nuclear test. *Seismological Research Letters*, *85*(1), 130–134. <https://doi.org/10.1785/0220130103>
- Zhao, L. F., Xie, X. B., Wang, W. M., Zhang, J. H., & Yao, Z. X. (2010). Seismic Lg-wave Q tomography in and around Northeast China. *Journal of Geophysical Research*, *115*(B8). <https://doi.org/10.1029/2009jb007157>
- Zhao, L. F., Xie, X. B., Wang, W. M., Zhang, J. H., & Yao, Z. X. (2013). Crustal Lg attenuation within the North China Craton and its surrounding regions. *Geophysical Journal International*, *195*(1), 513–531. <https://doi.org/10.1093/gji/ggt235>
- Zheng, X. F., Yao, Z. X., Liang, J. H., & Zheng, J. (2010). The role played and opportunities provided by IGP DMC of China National Seismic Network in Wenchuan earthquake disaster relief and researches. *Bulletin of the Seismological Society of America*, *100*(5B), 2866–2872. <https://doi.org/10.1785/0120090257>